

CONSTRAINTS ON QUINTESSENCE FROM FUTURE GALAXY CLUSTER SURVEYS

ZOLTÁN HAIMAN^{1,2,3}, JOSEPH J. MOHR^{4,5} & GILBERT P. HOLDER⁵

²Princeton University Observatory, Princeton, NJ

³NASA/Fermilab Astrophysics Center, Fermi National Accelerator Laboratory, Batavia, IL

⁵Department of Astronomy and Astrophysics, University of Chicago, Chicago, IL

Submitted to ApJ, February 15, 2000

ABSTRACT

We study the expected redshift evolution of galaxy cluster abundance between $0 \lesssim z \lesssim 3$ in different cosmologies, including the effects of the cosmic equation of state parameter $w \equiv p/\rho$. Using the Press–Schechter formalism, we model the expected cluster yields in a 12 deg^2 Sunyaev-Zel’dovich Effect (SZE) survey and a deep 10^4 deg^2 X-ray survey over a wide range of cosmological parameters. We quantify differences among cosmologies using both the total number and redshift distribution of clusters.

Provided that the local cluster abundance is known to a few percent accuracy, we find only mild degeneracies between w and either Ω_m or h . As a result, both surveys will provide improved constraints on w . The Ω_m – w degeneracy from the SZE survey lies nearly orthogonal to those found in studies of CMB anisotropy or high-redshift Supernovae (SNe). Using the SZE survey together with either CMB or SNe studies will determine both w and Ω_m to $\approx 3\%$ (68% confidence). The large number of clusters in the X-ray survey substantially reduces the degeneracy between w and both Ω_m and h , enabling measurements of w to $\approx 8\%$ and Ω_m to $\approx 1\%$ accuracy without relying on either the CMB or SNe data. The measured temperatures within the X-ray sample should provide a handle on possible systematic uncertainties, such as the redshift-evolution of internal cluster structure.

Subject headings: cosmology: theory – cosmology: observation

1. INTRODUCTION

It has long been realized that clusters of galaxies provide a uniquely useful probe of the fundamental cosmological parameters. The formation of the large-scale dark matter (DM) potential wells of clusters is likely independent of complex gas dynamical processes, star formation, and feedback, and involve only gravitational physics. As a result, the abundance of clusters N_{tot} and their distribution in redshift dN/dz should be determined purely by the geometry of the universe and the power spectrum of initial density fluctuations. Exploiting this relation, the observed abundance of nearby clusters has been found to constrain the amplitude of the power spectrum on cluster scales to an accuracy of $\sim 25\%$ (e.g. Viana & Liddle 1996). The value of σ_8 in these studies depends on the assumed underlying cosmology, especially on the density parameters Ω_m and Ω_Λ . Subsequent works (Bahcall & Fan 1998, Blanchard & Bartlett 1998, Viana & Liddle 1999) have shown that the redshift-evolution of the observed cluster abundance already places useful constraints on these two cosmological parameters.

In the above studies, the equation of state for the Λ -component has been implicitly assumed to be $p = w\rho$ with $w = -1$. The recent suggestion that w might be different from -1 , or even redshift dependent (Caldwell, Dave & Steinhardt 1998) has inspired several studies of the so-called “quintessence” cosmologies. From a particle physics point of view, such $w > -1$ can arise in a number of theories (see Turner & White 1997, Caldwell, Dave & Steinhardt 1998 and references therein). It is therefore of considerable interest to search for possible astrophysical

signatures of these equations of state, especially those that distinguish $w = -1$ from $w > -1$. Wang et al. (2000) has summarized current astrophysical constraints that suggest $-1 \leq w \lesssim -0.2$.

The galaxy cluster abundance provides a natural test of “quintessence” models, because w directly affects the growth of fluctuations D_z and the volume element $dV/dz d\Omega$. Furthermore, because of the dependence of the angular diameter distance d_A on w , the experimental detection limits for individual clusters, e.g., from the Sunyaev–Zel’dovich effect (SZE) decrement or the X-ray luminosity, depend on w . Wang & Steinhardt (1998, hereafter WS98) studied the constraints on w from a combination of measurements of the cluster abundance and Cosmic Microwave Background (CMB) anisotropies. Their work has shown that the slope of the comoving abundance dN/dz between $0 < z < 1$ depends sensitively on w , an effect that can break the degeneracies between w and combinations of other parameters (h, Ω, n) in the CMB anisotropy alone.

Here we consider in greater detail the constraints on w from cluster abundance evolution. Our main goals are: (1) to quantify the accuracy to which $w \neq -1$ models can be distinguished from standard Λ Cold Dark Matter (CDM) cosmologies using cluster abundance evolution; (2) to assess these accuracies in two specific proposed cluster surveys: an SZE survey (Carlstrom et al. 1999) and a wide area X-ray survey, and (3) to contrast constraints from cluster abundance to those from CMB anisotropy measurements and from luminosity distances to high-redshift Supernovae (Schmidt et al. 1998, Perlmutter et al. 1999).

¹Hubble Fellow

⁴Chandra Fellow

Our work differs from the analysis of WS98 in several ways. We examine the surface density of clusters $dN/dz d\Omega$, rather than the comoving number density $n(z)$. This is important from the observational point of view, because the former, directly measurable quantity inevitably includes the additional cosmology-dependence from the volume element $dV/dz d\Omega$. We incorporate the mass-limits expected from both types of surveys. Because the SZE survey has a nearly z -independent sensitivity, we find that high-redshift clusters at $z > 1$ yield useful constraints, in addition to those studied by WS98 in the range $0 < z < 1$. Finally, we quantify the statistical significance of differences in the models by applying a combination of a KS and a Poisson test to $dN/dz d\Omega$, and obtain constraints using a grid of models for a wide range of cosmological parameters.

This paper is organized as follows. In § 2, we describe the main features of the forthcoming SZE and X-ray surveys relevant to this work; and in § 3 we briefly summarize our modeling methods and assumptions. In § 4, we quantify the effect on w and other parameters on cluster abundance and evolution, and in § 5, we obtain the constraints on w by considering a grid of different cosmological models. In § 6, we discuss our results and the implications of this work, and in § 7, we summarize our conclusions.

2. FUTURE CLUSTER SURVEYS

The observational samples available for studies of cluster abundance evolution will improve enormously over the coming decade. The present samples of tens of intermediate redshift clusters (e.g., Gioia et al. 1990, Vikhlinin et al. 1998) will be replaced by samples of thousands of intermediate redshift and hundreds of high redshift ($z > 1$) clusters. At a minimum, the analysis of the European Space Agency X-ray Multi-mirror Mission (XMM) archive for serendipitously detected clusters will yield hundreds, and perhaps thousands of new clusters with emission weighted mean temperature measurements (Romer et al. 2000). Proposed X-ray and SZE surveys could likely surpass the XMM sample in areal coverage, number of detected clusters or redshift depth. The imminent improvement of distant cluster data motivates us to estimate the cosmological power of these future surveys. Note that in practice, the only survey details we utilize in our analyses are the virial mass of the least massive, detectable cluster (as a function of redshift and cosmological parameters), and the solid angle of the survey. We include here a brief description of the surveys for completeness.

2.1. A Sunyaev-Zel'dovich Effect Survey

The SZE survey we consider is that proposed by Carlstrom and collaborators (Carlstrom et al. 1999). This interferometric survey is particularly promising, because it will detect clusters more massive than $\sim 2 \times 10^{14} M_{\odot}$, nearly independent of their redshift. Combined, this low mass threshold and its redshift independence produce a cluster sample which extends, depending on cosmology, to redshifts $z \sim 3$. The proposed survey will cover 12 deg^2 in a year; it will be carried out using ten 2.5 m telescopes and an 8 GHz bandwidth digital correlator operating at cm wavelengths (Mohr et al. 1999). The detection limit as a function of redshift and cosmology $M_{\min}(z, \Omega_m, h)$ for this survey has been studied using mock observations of

simulated galaxy clusters (Holder et al. 2000), and we draw on those results here.

Optical and near infrared followup observations will be required to determine the redshifts of SZE clusters. Given the relatively small solid angle of the survey, it will be straightforward to obtain deep, multiband imaging. We expect that the spectroscopic followup will require access to a multiobject spectrograph on a 10 m class telescope. The ongoing development of infrared spectrographs may greatly enhance our ability to effectively estimate redshifts for the most distant clusters detected in the SZE survey.

2.2. A Deep, Wide-area X-ray Survey

We also consider the cosmological sensitivity of a wide area, deep X-ray imaging survey. The characteristics of our survey are drawn from a mission under consideration for the NASA ‘‘Small Explorers’’ program. The survey depth is $3.6 \times 10^6 \text{ cm}^2\text{s}$ at 1.5 keV, and the coverage is 10^4 deg^2 (approximately half the available unobscured sky). We assume that the imaging characteristics of the survey are sufficient to allow separation of the 10% clusters from the 90% AGNs and galactic stars. We focus on clusters which produce 500 detected source counts in the 0.5:6.0 keV band, sufficient to reliably estimate the emission weighted mean temperature in a survey of this depth (the external and internal backgrounds sum to $\sim 1.4 \text{ cts/arcmin}^2$).

To compute the number of photons detected from a cluster of a particular flux, we assume the clusters emit Raymond-Smith spectra (Raymond & Smith 1977) with $\frac{1}{3}$ solar abundance, and we model the effects of Galactic absorption using a constant column density of $N_H = 4 \times 10^{20} \text{ cm}^{-2}$. We assume that the detectors have a quantum efficiency similar to the ACIS detectors (Bautz et al. 1998, Chartas et al. 1998) on the Chandra X-ray Observatory, and the energy dependence of the mirror effective area mimics that of the mirror modules on ABRIXAS (Friedrich et al. 1998).

The X-ray survey could be combined with the Sloan Digital Sky Survey (SDSS) to obtain redshifts for the clusters – the redshift distribution of the clusters which produce 500 photons in the survey described above is well matched to the SDSS photometric redshift limit.

2.3. Determining the Survey Limiting Mass M_{\min}

For our analysis, the most important aspect of both surveys is the limiting mass $M_{\min}(z, \Omega_m, w, h)$, as a function of redshift and cosmological parameters. More specifically, we seek the relation between the detection limit of the survey, and the corresponding virial mass in the Press-Schechter formalism.

In the X-ray survey, M_{\min} follows from the cluster X-ray luminosity – virial mass relation and the details of the survey. We adopt the relation between virial mass and temperature promoted by Bryan & Norman (1998),

$$M = a \frac{T^{3/2}}{E(z) \sqrt{\Delta_c(z)}}, \quad (1)$$

where $H(z) = H_0 E(z)$ is the Hubble parameter, a is a normalization determined from the hydrodynamical simulations and Δ_c is the enclosed overdensity (relative to

the critical density) which defines the cluster virial region. The normalization a is found to be relatively insensitive to cosmological parameters, and the redshift evolution of Equation 1 appears to be consistent with the hydrodynamical simulations in those models where it has been tested (Bryan & Norman 1998). Here we assume that Equation 1 holds in all cosmologies with the same value of a , and use the fitting formulae for Δ_c provided by WS98, which includes the case $w \neq -1$. We then utilize Equation 1, together with the relation between bolometric luminosity and temperature found by Arnaud & Evrard (1999), to find the limiting mass of a cluster that produces 500 photons in the 0.5:6.0 keV band in a survey exposure. For these calculations we assume that the luminosity-temperature relation does not evolve with redshift, consistent with the currently available observations (Mushotzky & Scharf 1997).

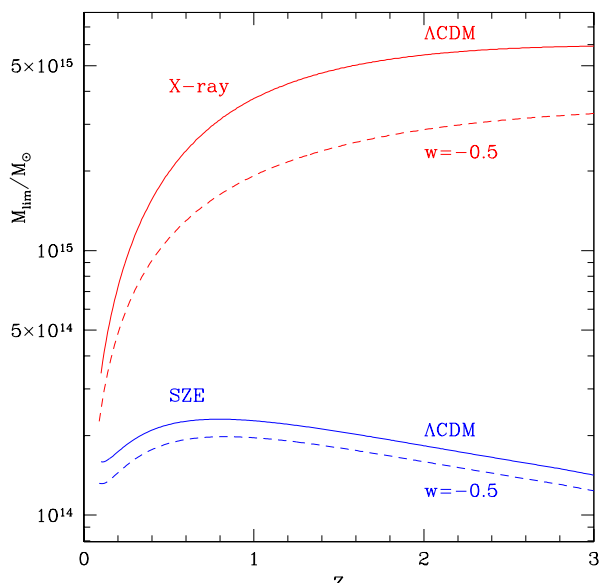


FIG. 1.— Limiting cluster virial masses for detection in the X-ray survey (upper pair of curves) and in the SZE survey (lower pair of curves). The solid curves show the mass limit in our fiducial flat Λ CDM model, with $w = -1$, $\Omega_m = 0.3$, and $h = 0.66$, and the dotted curves show the masses in the same model except with $w = -0.5$.

For an interferometric SZE survey, the relevant observable is the cluster visibility V , which is the Fourier transform pair of the cluster SZE brightness distribution on the sky as seen by the interferometer. The visibility is proportional to the total SZE flux decrement S_ν ,

$$V \propto S_\nu(M, z) \propto f_{ICM} \frac{M \langle T_e \rangle_n}{d_A^2} \quad (2)$$

where $\langle T_e \rangle_n$ is the electron density weighted mean temperature, M is the virial mass, f_{ICM} is the intracluster medium mass fraction and d_A is the angular diameter distance. We normalize this relation using mock observations of numerical cluster simulations (e.g., Mohr & Evrard 1997, Mohr, Mathiesen & Evrard 1999) carried out in three different cosmological models, including noise characteristics appropriate to the proposed SZE array (see Holder et al. 2000 for more details). The ICM mass fraction is set to $f_{ICM} = 0.2$ in all three cosmological models.

Note that for a flux limited survey, the limiting mass in equation 2 is sensitive to cosmology through its depen-

dence on d_A and the virial mass M . In the Press–Schechter formalism (see below), the virial mass corresponds to a region of enclosed overdensity with respect to critical density of $\Delta_c = 178$ in standard CDM, but it is lower and redshift-dependent in other cosmologies. We adopt the simulation normalized value of $M_{\min}^*(z)$ in our fiducial cosmology as a template, and then we rescale this relation to determine $M_{\min}(z)$ in the model of interest using the relation

$$M_{\min}(z) = M_{\min}^*(z) \frac{h^*}{h} \left[\frac{d_A(z)}{d_A^*(z)} \right]^{6/5} \left[\frac{\Delta_c^*(z)}{\Delta_c(z)} \right]^{1/2} \quad (3)$$

Here the superscript $*$ refers to quantities in the Λ CDM reference cosmology, and we have used the scaling of virial mass with temperature (Eqn. 1): $M \propto \langle T_e \rangle_n^{3/2}$, and the last factor accounts for the cosmological dependence of the virial mass. We have tested this scaling by comparing it to mock observations in simulations of two different cosmologies (open CDM and standard CDM), and found that agreement was better than $\sim 10\%$ in the redshift range $0 < z < 3$.

The mass limits we derived for both surveys are shown in the redshift range $0 < z < 3$ in Figure 1, both for Λ CDM and for a $w = -0.5$ universe. The SZE mass limit is nearly independent of redshift, and changes little with cosmology. As a result, the cluster sample can extend to $z \approx 3$. In comparison, the X-ray mass limit is a stronger function of w , and it rises rapidly with redshift. For the X-ray survey considered here the number of detected clusters beyond $z \approx 1$ is negligible.

These mass limits admittedly incorporate some simplifying assumptions that have not been tested in detail. Our goal was to capture the scaling with cosmological parameters and redshift as best as possible. However, we emphasize that further studies of the sensitivities of these scalings to, for example, energy injection during galaxy formation will be critical to interpreting the survey data. In the case of the X-ray survey, the cluster sample will have measured temperatures, allowing the limiting mass to be estimated directly from data. In the case of the SZE survey, deep X-ray followup or multifrequency SZE followup observations should yield direct measurements of the limiting mass.

3. ESTIMATING CLUSTER ABUNDANCE

We assume that the comoving number density $(dn/dM)dM$ of clusters at redshift z with mass $M \pm dM/2$ is given by the Press–Schechter formula (Press & Schechter 1974),

$$\frac{dn}{dM}(z, M) = \sqrt{\frac{2}{\pi}} \frac{\rho_0}{M} \frac{\delta_c}{D_z \sigma_M^2} \frac{d\sigma_M}{dM} \exp\left(-\frac{\delta_c^2}{2D_z^2 \sigma_M^2}\right), \quad (4)$$

where σ_M is the r.m.s. density fluctuation, computed on mass-scale M from the present-day linear power spectrum (Eisenstein & Hu 1998), D_z is the linear growth function, ρ_0 is the present-day mass density, and $\delta_c \approx 1.68$ is the linear threshold overdensity for collapse. The Press–Schechter formalism has been shown to be in reasonably good agreement with results from N-body simulations (Lacey & Cole 1994, Gross et al 1998, Lee & Shandarin 1999). The directly observable quantity, i.e. the average number of clusters with mass above M_{\min} at redshift

$z \pm dz/2$ observed in a solid angle $d\Omega$ is then simply given by

$$\frac{dN}{dzd\Omega}(z) = \left[\frac{dV}{dzd\Omega}(z) \int_{M_{\min}(z)}^{\infty} dM \frac{dn}{dM} \right] \quad (5)$$

where $dV/dzd\Omega$ is the cosmological volume element, and $M_{\min}(z)$ is the limiting mass as discussed in section 2.3. Equations 4 and 5 depend on the cosmological parameters through ρ_0 , D_z , and $dV/dzd\Omega$, in addition to the mild dependence of σ_M on these parameters through the power spectrum (although the dependence on the power-spectrum is more pronounced in the X-ray survey, where the limiting mass varies strongly with redshift). Note that the comoving abundance dn/dM is exponentially sensitive to the growth function D_z . We use convenient expressions for $dV/dzd\Omega$ and D_z in open and flat Ω_Λ cosmologies available in the literature (Peebles 1980, Carroll, Press & Turner 1992, Eisenstein 1996). In the case of cosmologies with $w \neq -1$, we have evaluated $dV/dzd\Omega$ numerically, but used the fitting formulae for D_z obtained by WS98, which are valid for constant or slowly-changing w 's. It is generally found that δ_c does not vary significantly with cosmology (e.g., Lacey & Cole 1993); here we simply assume $\delta_c = 1.68$ in all cosmologies, which gives an agreement with simulations to within a factor of ≈ 2 (although small modifications to δ_c can give even better agreement, see Lacey & Cole 1994, Bond & Myers 1996).

3.1. Normalizing to Local Cluster Abundance

To compute $dN/dzd\Omega$ from equation 5, we must choose a normalization σ_8 for the density fluctuations on cluster scales, where σ_8 is the present epoch, linearly extrapolated *rms* variation in the density field filtered on scales of $8h^{-1}$ Mpc. To be consistent in our analysis, we choose the normalization for each cosmology by fixing the local cluster abundance above a given mass $M_{\text{nm}} = 10^{14}h^{-1} M_\odot$. In all models considered, we set the local abundance to be $1.5 \times 10^{-5} (h/0.66)^3 \text{ Mpc}^{-3}$, the value derived in our fiducial Λ CDM model (see below). We have chosen to normalize using the local cluster abundance (upto a factor h^3) above mass M_{nm} rather than above a particular emission weighted mean temperature kT_{nm} , because this removes the somewhat uncertain cosmological sensitivity of the virial mass temperature ($M - T_x$) relation from the normalization process; spherical tophat calculations suggest a significant offset in the $M - T_x$ normalization of the open and flat $\Omega_m = 0.3$ models which hydrodynamical simulations do not seem to reproduce (Evrard, Metzler & Navarro 1996, Bryan & Norman 1998, Viana & Liddle 1999).

Our normalization approach is sensible, because the number density of nearby clusters can be measured to within a factor of h^3 , and the masses of nearby clusters can be measured directly through several independent means; these include the assumption of hydrostatic equilibrium and using X-ray images and intracluster medium (ICM) temperature profiles, weak lensing, or galaxy dynamical mass estimates. The only cosmological sensitivity of these mass estimators is their dependence on the Hubble parameter h ; we include this h dependence when normalizing our cosmological models. Note that previous derivations of σ_8 (e.g. Viana & Liddle 1993; Pen 1998) in various cosmologies from the local cluster abundance $N(> kT)$ above

a threshold temperature $kT_{\min} \sim 7\text{keV}$ found a scaling $\sigma_8 \Omega_m^{1/2} \approx 0.5$. Since our normalization is based on mass, rather than temperature, in general, we find a different scaling (if a ~ 5 times smaller threshold temperature is used, the constrained combination is already quite different, $\sigma_8 \Omega_m \sim \text{constant}$).

3.2. Fiducial Cosmological Model

The parameters we chose for our fiducial cosmological model are $(\Omega_\Lambda, \Omega_m, h, \sigma_8, n) = (0.7, 0.3, 0.66, 1, 1)$. This flat Λ CDM model is motivated as a “best-fit” model that produces a local cluster abundance consistent with observations (Viana & Liddle 1999), and satisfies the current constraints from CMB anisotropy, high- z SNe, and other observations (Bahcall et al. 1999). We have assumed a baryon density of $\Omega_b h^2 = 0.0193$, consistent with recent D/H measurements (e.g. Burles & Tytler 1998). Note that the power spectrum index n is not important for the analysis presented here, because we normalize on cluster scales σ_8 , and we find that this minimizes the effect of varying n on the density fluctuations relevant to cluster formation.

4. EFFECT OF EQUATION OF STATE ON CLUSTER ABUNDANCE EVOLUTION

In this section, we describe how variations of the individual parameters Ω , h , and w affect the cluster abundance and redshift distribution. This will be useful in understanding the results of the next section, when a full grid of different cosmologies is considered. In addition, we describe our method of quantifying the statistical significance of differences between the distributions dN/dz in a pair of different cosmologies.

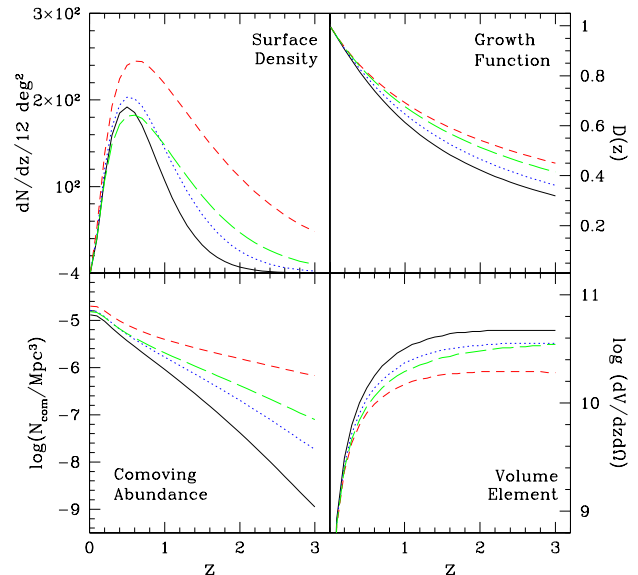


FIG. 2.— Effect of changing w when all other parameters are held fixed. The four panels show (clockwise from upper left) the surface density of clusters at redshift z ; the linear growth function; the volume element in units of $\text{Mpc}^3 \text{sr}^{-1} \text{redshift}^{-1}$; and the comoving cluster abundance. The solid curve shows our fiducial flat Λ CDM model, with $w = -1$, $\Omega_m = 0.3$, and $h = 0.66$. The dotted curve is the same model with $w = -0.6$, the short-dashed curve with $w = -0.2$, and the long-dashed curve is an open CDM model with $\Omega_m = 0.3$.

4.1. Single Parameter Variations

The surface density of clusters more massive than M_{\min} depends on the assumed cosmology mainly through the growth function $D(z)$ and volume element $dV/dz d\Omega$. In the approach described in section 3, once a cosmology is specified, the normalization of the power spectrum σ_8 is found by keeping the abundance of clusters at $z = 0$ constant. We therefore consider only three “free” parameters, w , h , Ω_m , specifying the cosmology. We assume the universe to be either flat ($\Omega_Q = 1 - \Omega_m$), or open with $\Omega_Q = 0$.

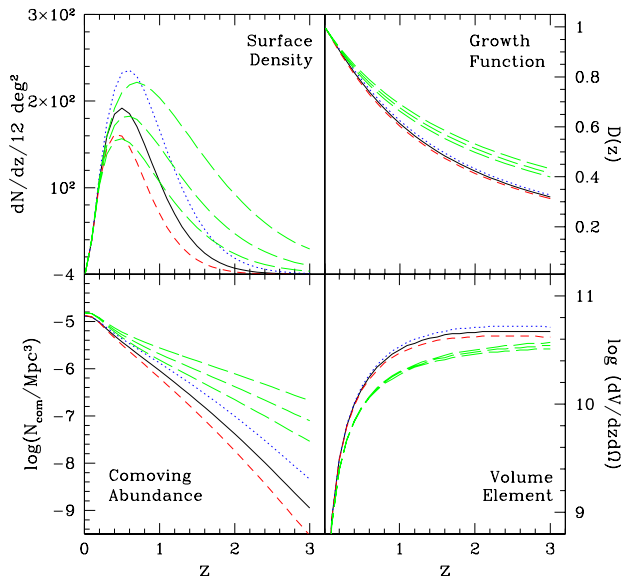


FIG. 3.— Effect of changing Ω_m when all other parameters are held fixed. The Λ CDM model of Figure 2 is shown (solid curve) together with models with $\Omega = 0.27$ (dotted curve); $\Omega = 0.33$ (short-dashed curve); and OCDM models with $\Omega = 0.27, 0.30, 0.33$ (long-dashed curves, top to bottom).

Changing w . The effects of changing w are demonstrated in Figure 2. The top left panel shows the total number of clusters in a 12 square degree field, detectable down to the constant SZE decrement S_{\min} . As discussed in section 2.3 above, a constant S_{\min} implies a redshift and cosmology-dependent limiting mass M_{\min} ; in general, we find that including this effect somewhat reduces our sensitivity to w (see Figure 5 and discussion below). Figure 2 shows models with ($\Omega_m = 0.3, h = 0.66$) and with three different w 's: $w = -1$ (solid curve), $w = -0.6$ (dotted curve), and $w = -0.2$ (short-dashed curve). In addition, we show the result from an open CDM model with ($\Omega = 0.3, h = 0.66$, long-dashed curve). This panel reveals that increasing w from $w = -1$ causes the slope of the redshift distribution above $z \approx 0.5$ to flatten, increasing the number of high- z clusters. Furthermore, “opening” the universe has an effect similar to increasing w . The other three panels demonstrate the reason for these scalings. The top right panel shows that the growth function is flatter in higher w models, significantly increasing the comoving number density of high-redshift clusters (bottom left panel). The volume element has the opposite behavior (bottom right panel), and it tends to balance the increase in the comoving abundance caused by the growth function in the range $0 < z \lesssim 0.5$; but for higher redshifts, the growth function “wins”. An important conclusion seen from Figure 2 is that both the total number of clusters as

well as the shape of their redshift distribution, significantly depends on w .

Changing Ω_m . The effects of changing Ω_m are shown in Figure 3. The curves correspond to a flat Λ CDM universe with ($h = 0.66, w = -1$), and $\Omega_m = 0.27$ (dotted), $\Omega_m = 0.30$ (solid), and $\Omega_m = 0.33$ (short-dashed). In addition, the long-dashed curves show the same three models (top to bottom), assuming open CDM with $\Omega_\Lambda = 0$. Several conclusions can be drawn from these plots. Overall, the top left panel shows that a decrease in Ω_m increases the number of clusters (and vice versa) at all redshifts. Note that the dependence is strong, for instance, a 10% decrease in Ω_m increases the total number of clusters by $\sim 25\%$ in either Λ CDM or OCDM cosmologies. As emphasized by Bahcall & Fan (1998), Viana & Liddle (1999) and others, this makes it possible to estimate an upper limit on Ω_m using current data on cluster abundances (i.e. a few high- z clusters). A second important feature seen in the top left panel is that the shape of the redshift distribution is not changed significantly, a conclusion that holds both in Λ CDM and OCDM. Finally, the remaining three panels reveal that the effects of Ω_m arise mainly from the changes in the comoving abundance (bottom left panel). In flat Λ CDM, Ω_m has relatively little effect on the volume or the growth function, and the comoving abundance is determined by the value of σ_8 that keeps the local abundance constant at $z = 0$ (we find $\sigma_8 = 0.93$ for $\Omega_m = 0.33$ and $\sigma_8 = 1.09$ for $\Omega_m = 0.27$). In addition, we find that the change in the shape of the underlying power spectrum with Ω_m enhances this effect. Unlike in the case of w , the volume element and the comoving abundance now act in the same direction: a lower Ω_m increases both the comoving abundance and the volume element. Note that in OCDM, the growth function has a larger effect, and that relative to Λ CDM, the redshift distribution is much flatter.

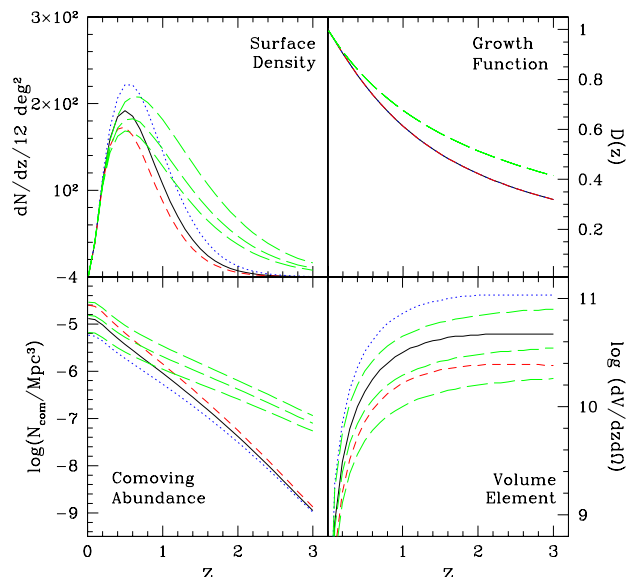


FIG. 4.— Effect of changing h when all other parameters are held fixed. The Λ CDM model of Figure 2 is shown (solid curve) together with models with $h = 0.5$ (dotted curve); $h = 0.82$ (short-dashed curve); and OCDM models with $h = 0.5, 0.66, 0.82$ (long-dashed curves, top to bottom).

Changing h . Figure 4 demonstrates the effects of changing h . Three Λ CDM models are shown with ($\Omega_m = 0.30, w = -1$), and $h = 0.5$ (dotted curve), $h = 0.66$ (solid curve), and $h = 0.82$ (short-dashed curves). The long-dashed curves correspond to OCDM models with the same parameters (top to bottom). Comparing the top right panel with that of Figure 3, the qualitative behavior of dN/dz under changes in h and Ω_m are similar: decreasing h increases the total number of clusters, but does not considerably change their redshift distribution. However, the sensitivity to h is significantly less: the total number of clusters is seen to increase by $\sim 25\%$ only when h is decreased by the same percentage. Note that the growth function is not effected by h , and the h sensitivity is driven by our normalization process, which fixes the abundance at $z = 0$ (see § 3.1). Since the volume scales as $\propto h^{-3}$, we fix the comoving abundance to be proportional to $\propto h^3$. As a result, $dN/dz d\Omega$ is nearly independent of h (e.g. for a pure power-law spectrum, there would be no h -dependence).

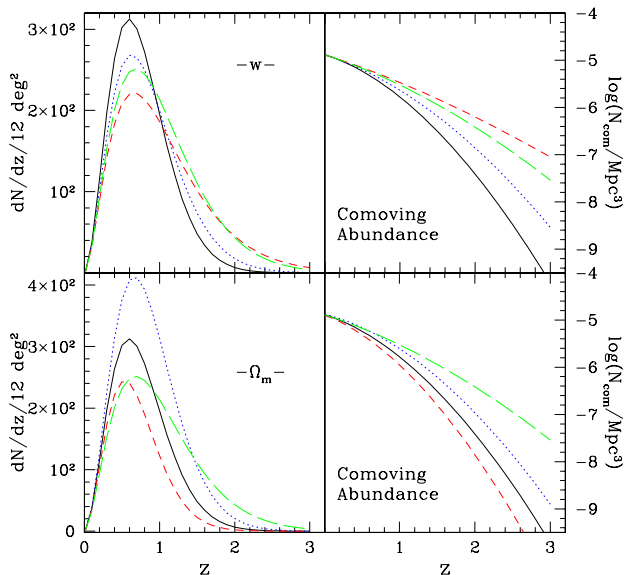


FIG. 5.— Effect of changing w (upper panels) or Ω_m (lower panels) when all other parameters are held fixed, including the mass limit. The types of the curves correspond to the different models, as shown in Figs 2 & 3.

Effects of M_{\min} . Finally, we examine the extent to which the above conclusions depend on the cosmology and redshift-dependence of the limiting mass M_{\min} . To do this, we compute cluster abundances above the fixed mass $M_{\min} = 10^{14} h^{-1} M_{\odot}$, characteristic of the SZE survey detection threshold in the range of cosmologies and redshifts considered here. The results are shown in Figure 5: the top panels show the surface density and comoving abundance when w is changed (the cosmological models are the same as in Figure 2), and the bottom panels show the same quantities under changes in Ω_m (the models are the same as in Figure 3). A comparison between Figures 5 and 2 gives an idea of the effects of the mass limit. The general trend seen in Figure 2 remains true, i.e. increasing w flattens the redshift distribution at high- z . However, when a constant M_{\min} is assumed, the “pivot point” moves to slightly higher redshift, and the total number of clusters becomes less sensitive to w . Similar conclusions can be drawn from a comparison of Figure 3 with the bottom two

panels of Figure 5: under changes in Ω_m the general trends are again similar, but the differences between the different models are amplified when a constant M_{\min} is used.

Abundances in the X-ray Survey. In Figure 6, we show the evolution of the cluster abundance, and its sensitivity to w and Ω_m , in the X-ray survey. Because of the much larger solid angle surveyed, the numbers of clusters is significantly larger than in the SZE case, despite the higher limiting mass (cf. Fig 1). Nevertheless, the trend that can be identified in the X-ray sample are similar to those in the SZE case. Raising w increases the total number of clusters, and flattens their redshift distribution. On the other hand, raising Ω_m decreases the total number of clusters. Note that in comparison to the SZE survey, Ω_m has a smaller effect on the total number, and a somewhat larger effect on the slope of the redshift distribution – these are caused by the stronger cosmology-dependence of the X-ray mass limit.

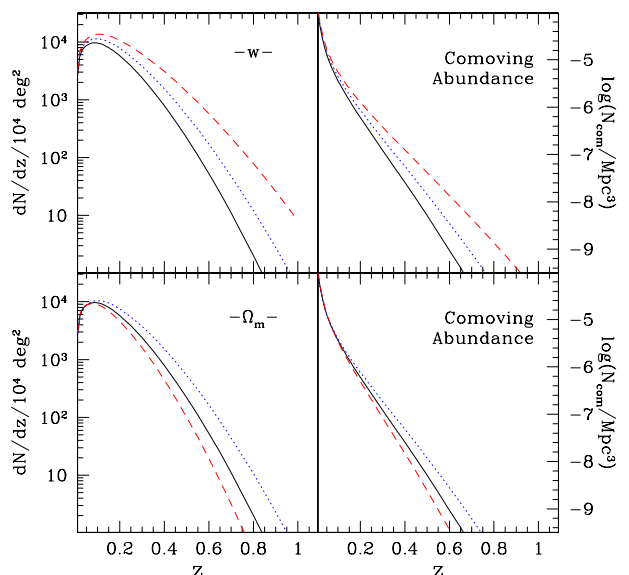


FIG. 6.— Effect of changing w (upper panels) or Ω_m (lower panels) when all other parameters are held fixed in an X-ray survey. Note the much larger numbers of clusters in comparison to the SZE survey. In the top panel, the curves correspond to $w = -1$ (solid), $w = -0.8$ (dotted) and $w = -0.6$ (dashed). In the bottom panel, the curves correspond to $\Omega_m = 0.3$ (solid), $\Omega_m = 0.27$ (dotted) and $\Omega_m = 0.33$ (dashed).

In summary, we conclude that changes in w modify both the normalization and the shape of the redshift distribution of clusters, while changes in Ω_m or h effect essentially only the overall amplitude. This suggests that changes in w can not be fully degenerate with changes in either Ω_m or h (or a combination), making it possible to measure w from cluster abundances alone. These conclusions hold either for clusters above a fixed detection threshold in and SZE or X-ray survey, or for a sample of clusters above a fixed mass.

4.2. Comparing dN/dz in Two Different Cosmologies

The main goal of this paper is to quantify the accuracy to which w can be measured in future SZE and X-ray surveys. To do this, we must answer the following question: given a hypothetical sample of N_{tot} clusters (with measured redshifts) obeying the distribution dN_A/dz of

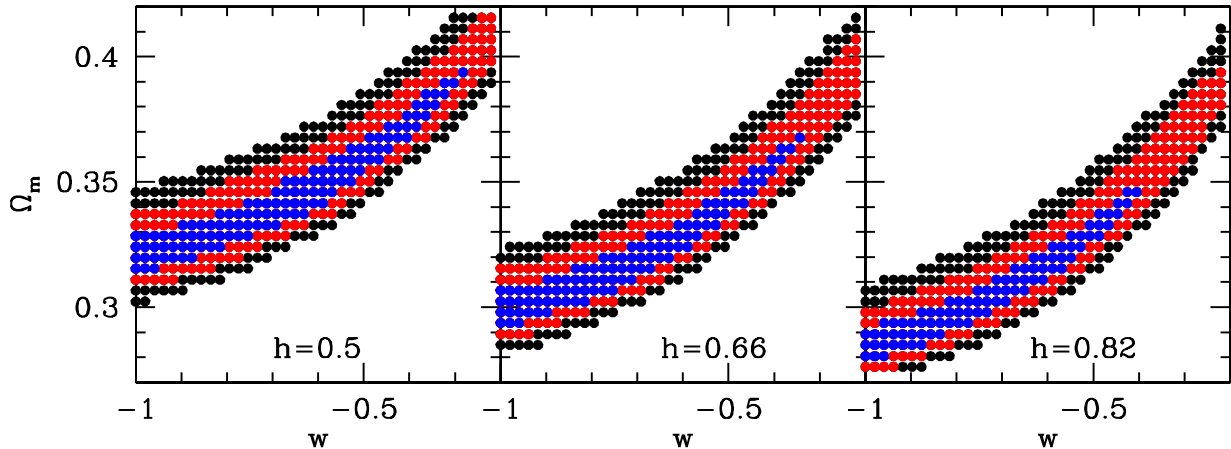


FIG. 7.— Contours of 1, 2, and 3σ significance for different models when they are compared to a fiducial flat Λ CDM model with $\Omega_m = 0.3$ and $h = 0.66$, using the SZE survey. The three panels show three different cross-sections of constant total probability at fixed values of h (0.5, 0.66, and 0.82) in the investigated 3-dimensional Ω_m, h, w parameter space.

the test model (A) cosmology, what is the probability $P_{\text{tot}}(A, B)$ that the same sample of clusters is detected in the fiducial (B) cosmology, with distribution dN_B/dz ? We have seen in section 4.1 that the overall amplitude, and the shape of dN/dz are both important. Motivated by this, we define

$$P_{\text{tot}}(A, B) = P_0(A, B) \times P_z(A, B) \quad (6)$$

where $P_0(A, B)$ is the probability of detecting $N_{A,\text{tot}}$ clusters when the mean number is $N_{B,\text{tot}}$, and $P_z(A, B)$ is the probability of measuring the redshift distribution of model (A) if the true parent distribution is that of model (B). We assume P_0 is given by the Poisson distribution, and we use the Kolmogorov–Smirnov (K–S) test to compute $P_z(A, B)$ (Press et al. 1992). With this approach (as opposed to the usual χ^2 tests), we need not bin the data in redshift.

For reference, it is useful to quote here some examples for the probabilities, taking ($\Omega_m = 0.3, h = 0.66, w = -1$) as the fiducial (B) model. For example, closest to this model in Figure 2 is the one with $w = -0.6$. For this case, we find $P_0 = 6 \times 10^{-5}$ and $P_z = 3.5 \times 10^{-3}$ for a total probability of $P_{\text{tot}} = 2.1 \times 10^{-7}$. In other words, the two cosmologies could be distinguished at a likelihood of 4σ using only the total number of clusters, at 2.9σ using only the shape of the redshift distribution, and at the 5.2σ level using both pieces of information. Taking the $\Omega_m = 0.33$ Λ CDM cosmology from Figure 3 as another example for model (A), we find $P_0 = 5.3 \times 10^{-4}$ ($=3.5\sigma$), $P_z = 4.2 \times 10^{-1}$ ($=0.8\sigma$), and a total probability of $P_{\text{tot}} = 2.2 \times 10^{-4}$ ($=3.9\sigma$). Not surprisingly, the shape does not add significantly to the constraint. An example where the opposite is true is the $\Omega_m = 0.33$ open CDM cosmology in Figure 3, for which we find $P_0 = 0.15$ ($=1.4\sigma$), $P_z = 7 \times 10^{-2}$ ($=1.8\sigma$), and a total probability of $P_{\text{tot}} = 0.01$ ($=2.6\sigma$). In this case, the distinction is made primarily by the different redshift distributions, rather than the total number of detected clusters.

5. CONSTRAINTS ON THE EQUATION OF STATE

We derive cosmological constraints by considering a 3-dimensional grid of models in Ω_m, h , and w . As described above, we first find σ_8 in each model, so that all models are normalized to produce the same local cluster abundance

at $z = 0$. We then compute $dN/dzd\Omega$ in these models for $0.2 \leq \Omega_m \leq 0.5$, $0.5 \leq h \leq 0.9$, and $-1 \leq w \leq -0.2$. The range for w corresponds to that allowed by current astrophysical constraints (Wang et al. 2000).

5.1. Expectations from the Sunyaev–Zel’dovich Survey

Figure 7 shows contours of 1, 2, and 3σ for the total probability P_{tot} for models when compared to the fiducial flat Λ CDM model. The three panels show three different cross-sections of the investigated 3-dimensional Ω_m, h, w parameter space, taken at constant values of $h = 0.5, 0.66$, and 0.82 , spanning the range of values preferred by other observations. The most striking feature in this figure is the direction of the contours, which turn upwards in the w, Ω_m plane, and become narrower for larger values of w . We find that the trough of maximum probability for fixed $h = 0.66$ is well described by

$$(\Omega_m - 0.3)(w + 1)^{-3/2} = 0.1, \quad (7)$$

with further constant shifts in Ω_m caused by changing h . The $\pm 3\sigma$ width enclosed by the contours around this relation is relatively narrow in Ω_m ($\pm 6\%$). In a Λ CDM case, even when a large range of values is considered for h , the constraint $0.27 \lesssim \Omega_m \lesssim 0.35$ would follow; when $w \neq -1$ is considered, the allowed range widens to $0.27 \lesssim \Omega_m \lesssim 0.45$. On the other hand, a wide range of w 's is seen to be consistent with $w = -1$: the largest currently allowed value, $w \approx -0.2$ is approximately 3σ away from $w = -1$, and $w = -0.6$ is allowed at 1σ . Note that h is not well determined, i.e. the contours look similar for all three values of h , and 1σ models exist for any value of h in the range $0.5 \lesssim h \lesssim 0.9$. This is not surprising, as Figure 4 shows $dN/dzd\Omega$ is sensitive to the value of h only through its effect on the determination of σ_8 .

5.2. Expectations from the X-ray Survey

Figure 8 contains expectations for the X-ray survey; we show contours of 1, 2, and 3σ probabilities relative to the fiducial Λ CDM model. The qualitative features are similar to that in the SZE case, but owing to the larger number of clusters, the constraints are significantly stronger: the

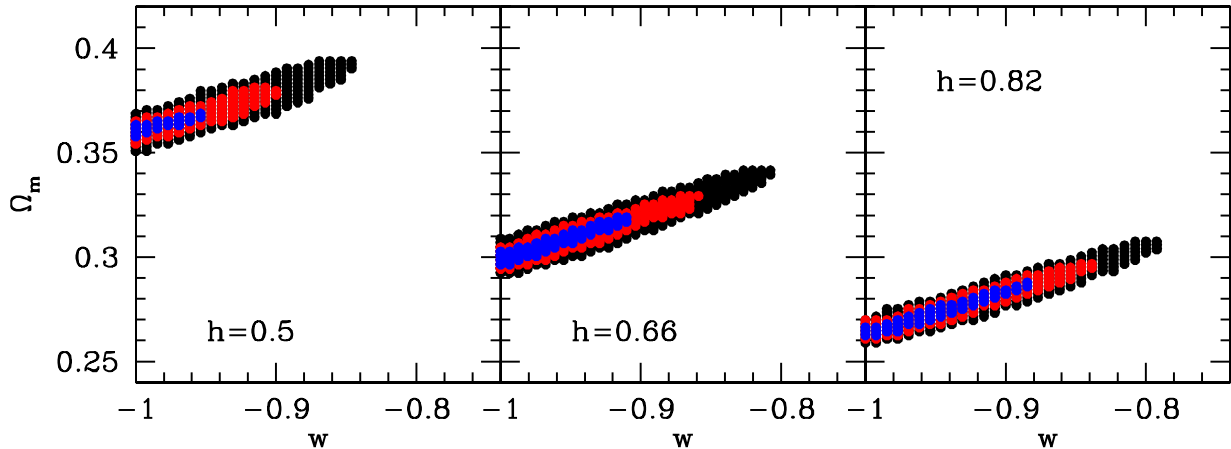


FIG. 8.— Contours of 1, 2, and 3σ probabilities for models when they are compared to a fiducial flat Λ CDM model, as in Figure 7, but for the X-ray survey.

contours are narrower, and do not extend to large values of w . Most importantly, the largest value of w allowed at a probability better than 3σ is $w \approx -0.8$, even assuming that the values of Ω_m and h are not known. Although the contours are narrower than in the SZE case, assuming that h and w are unknown, the allowed range of Ω_m is similar to that in the SZE case, $0.26 \lesssim \Omega_m \lesssim 0.39$. Note that a knowledge of h would not significantly improve this constraint (although if h is found to be low, then the lower limit in Ω_m would increase). Finally, assuming that both h and Ω_m are known to high accuracy, the allowed 3σ range on w would reduce to $-1 \leq w \lesssim -0.95$.

6. RESULTS AND DISCUSSION

6.1. Total Number vs. the Redshift Distribution

Our main results are presented in Figures 7 and 8, which show the probabilities of various models relative to a fiducial Λ CDM model. As demonstrated by these figures, the SZE survey determines only a combination of Ω_m and w ; in the absence of external constraints on Ω_m , w as large as -0.2 is only inconsistent with $w = -1$ at 3σ . On the other hand, the X-ray survey could distinguish a $w \approx -0.8$ or a $w \approx -0.95$ model from Λ CDM at 3σ significance, depending on whether Ω_m is known to high accuracy from other studies.

It is interesting to ask whether these constraints arise mainly from the total number of detected clusters, or from their redshift distribution. To address this issue, in Figure 9 we show separate probability contours for the probability P_0 (total number of clusters, left panels), and for the probability P_z (shape of redshift distribution, right panels). In the SZE case, the P_0 and P_z contours unfavorably run along nearly identical directions. At $w \lesssim -0.5$, the shape information plays almost no role (the contours of P_{tot} and P_0 are indistinguishable), but at $w \gtrsim -0.5$, the shape becomes increasingly important. At the largest values of $w \gtrsim -0.3$, the shape is a better discriminator for w than the total number of clusters. Note that the difference in shapes arises mostly from the high-redshift ($z \gtrsim 1$) clusters (cf. Fig. 2). As shown by the increased width of the contours in the bottom panels, Ω_m has a relatively small effect on the shape of the redshift distribution.

In the X-ray case (bottom panels in Fig. 9), the situ-

ation is different, because the contours of P_0 and P_z are both much narrower, and not nearly so parallel. As a result, the contours for the total probability do not reach beyond $w \approx -0.8$. Note that the redshift distribution (of clusters primarily in the $0 < z < 1$ range) here plays a crucial role. As Figures 4 and 3 show, the total number of clusters can be adjusted by changing Ω_m and h . In terms of the total number of clusters, w is therefore degenerate both with Ω_m and h : raising w lowers the total number, but this can always be offset by a change in Ω_m and/or h . The rightmost panel in the middle row of Fig. 8 reveals that based on P_0 alone, $w = -0.5$ (and $\Omega_m = 0.4$) can not be distinguished from Λ CDM even at the 1σ level. On the other hand, when the shape information is added, $w \lesssim -0.8$ follows to 3σ significance.

6.2. Caveats and Suggestions for Further Work

Our conclusions above are dependent on the chosen limiting mass, which is a function of both redshift and cosmology. We have attempted to include these dependencies, so that the whole cluster sample, down to the detection threshold is utilized. We have experimented with dN/dz distributions obtained when a *constant* mass limit is used at all redshifts and in all cosmologies. In general, we find that the shape of the redshift distribution is then a stronger function of w (cf. Fig. 2 and the top panels of Fig. 5). In principle, measured cluster velocity dispersions and X-ray temperatures (both cosmology independent) could be utilized to improve constraints on w , i.e. by using sub-samples that maximize the differences between models. Further work is needed to clarify the feasibility of this approach, as well as to confirm the expected dependence of M_{min} on Ω_m , h , w , and z .

Further work is required to test the cluster structural evolution models we used. For the X-ray survey, we have assumed that the cluster luminosity-temperature relation does not evolve, consistent with current observations (Mushotzky & Scharf 1997), and in the SZE survey, we have adopted the structural evolution found in state of the art hydrodynamical simulations (Holder et al. 2000). Because of the sensitivity of the survey yields to the limiting mass, cluster structural evolution which changes the observability of high redshift clusters can introduce systematic errors in cosmological constraints: for example,

both low Ω_m cosmologies and positive evolution of the cluster luminosity–temperature relation increase the cluster yield in an X-ray survey. SZE surveys are generally less sensitive to evolution than X-ray surveys, because the X-ray luminosity is heavily dependent on the core structure (e.g., the presence or absence of cooling instabilities), whereas the SZE visibility depends on the integral of the ICM pressure over the entire cluster (Eqn. 2). We are testing these assertions with a new suite of hydrodynamical simulations, in scenarios where galaxy formation at high redshift preheats the intergalactic gas before it collapses to form clusters (Evrard et al. in prep). Finally, we emphasize that because of the sensitivity of X-ray surveys to evolution, we have only used those clusters which produce enough photons to measure an emission weighted mean temperature. Using the measured temperatures, it should be possible to disentangle the cosmological effects from those caused by the evolution of cluster structure.

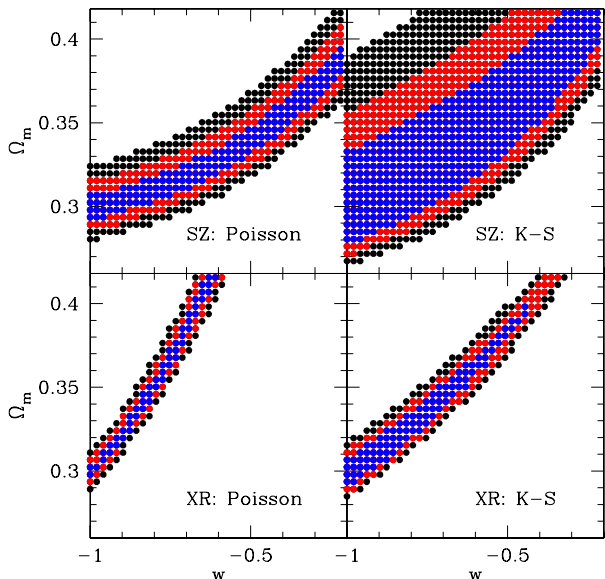


FIG. 9.— Probability contours of 1, 2, and 3σ probabilities as in Figures 7 and 8, but when only the total number of clusters (left panels), or only the redshift distributions (right panels) are used to compute the likelihoods between two models.

In our treatment, we have relied on the Press–Schechter formalism. In cosmologies where it has been tested against simulations, the number density of massive halos has been shown to agree with simulations to a factor of ~ 2 . It is critical to carry out comparisons between numerical simulations and Press–Schechter predictions for a wider range of cosmologies. Although we do not expect the results presented here to change qualitatively, changes in dN/dM by upto a factor of ~ 2 could affect the exact shape of the probability contours shown in Figures 7 and 8. We have further ignored the effects of galaxy formation and feedback on the limiting mass. In principle, the relation between the cluster SZE decrement and virial mass in the lowest mass clusters could be affected by these processes. In addition, the dependence of both the SZE decrement and the X-ray flux likely exhibits a non-negligible intrinsic scatter, which could effectively lower the limiting masses in our treatment, especially for the X-ray survey. The SZE decrement to virial mass relation is found to have a small scatter in numerical simulations (Metzler 1998), and

to cause a negligible increase in the total cluster yields (Holder et al. 1999).

Perhaps the most critical assumption is that the local cluster abundance is known to high accuracy. We have used this assumption to determine σ_8 , i.e. to eliminate one free parameter – effectively assigning “infinite weight” to the cluster abundance near $z = 0$. This approach is appropriate for several reasons. The cosmological parameters make little difference to the cluster abundance at $z \approx 0$, other than the volume being proportional to h^{-3} . Similarly, the study of local cluster masses is cosmologically independent (upto a factor of h). In a 10^4 square degree survey, we find that the total number of clusters between $0 < z < 0.1$, down to a limiting mass of $2 \times 10^{14} h^{-1} M_\odot$ is ≈ 4000 ; with a random error of only $\lesssim 2\%$. We have experimented with our models, assuming that the normalization at $z = 0$ can be increased/decreased by 2%, and found that a change at this level makes little difference to the probabilities between a pair of models.

It is nevertheless interesting to consider a different approach, where σ_8 is treated as another free parameter in addition to Ω_m , h , and w . As an example, we consider models with fixed $\Omega_m = 0.3$ and $h = 0.66$, and allow w to vary. At each w , we then determine the value of σ_8 that maximizes the total probability, (i.e. most similar to the fiducial model). We then find that models with $(w, \sigma_8) = (-0.6, 0.955)$, $(w, \sigma_8) = (-0.4, 0.905)$, and $(w, \sigma_8) = (-0.2, 0.860)$ differ from our fiducial $(w, \sigma_8) = (-1, -1)$ model at significances of 1σ , 2.5σ , and 4.2σ , respectively. These examples reveal that a mild degeneracy exists between w and σ_8 that might allow somewhat larger values of w than obtained by fixing σ_8 based on the local abundance. Note that in these models, the local abundance would, in fact, differ from that in the fiducial model by $\sim 10\%$, violating the local abundance constraint.

In section 5, we restricted our range of models to Λ CDM. We find that the redshift distribution of clusters in open CDM models typically resembles that in models with high w . This is demonstrated in Figure 2: both in the $w = -0.2$ and the OCDM model, the redshift distributions are flatter and extend to higher z than in Λ CDM. We find that OCDM models with suitably adjusted values of Ω_m and h are typically difficult to distinguish from those with $w \gtrsim -0.5$, but the flat shape of $dN/dz d\Omega$ makes OCDM easily distinguishable from Λ CDM. A broader study of different cosmological models, including those with both quintessence and curvature, time-dependent w , and those with non-Gaussian initial conditions could reveal new degeneracies, and will be studied elsewhere.

6.3. Clusters versus CMB Anisotropy and High- z SNe

A useful generic feature of the probability contours presented here is their difference from those expected in CMB anisotropy or Supernovae data. Two different cosmologies produce the same location (spherical harmonic index ℓ_{peak}) for the first Doppler peak for the CMB temperature anisotropy, provided they have the same comoving distance to the surface of last scattering (cf. Wang & Steinhardt 1998, White 1998, Huey et al. 1999). Note that this is only the most prominent constraint that can be obtained from the CMB data, with considerable more information once the location and height of the second and higher Doppler peaks are measured. Similarly; the appar-

ent magnitudes of the observed SNe constrain the luminosity distance $d_L(z)$ to $0 \leq z \lesssim 1$ (Schmidt et al. 1998, Perlmutter et al. 1999). In general, both of these types of observations will determine a combination of cosmological parameters that is different from the cluster constraints derived here.

In Figure 10, we zoom in on the relevant region of the $\Omega_m - w$ plane in the X-ray survey, and compare the cluster constraints to those expected from CMB anisotropy or high- z SNe. The three dashed curves correspond to the CMB constraints: the middle curve shows a combination of Ω_m and w that produces the constant $\ell_{\text{peak}} \approx 243$ obtained in our fiducial Λ CDM model (using the fitting formulae from White 1998 for the physical scale k_{peak}); the other two dotted curves bracket a $\pm 1\%$ range around this value. Similarly, the dotted curves correspond to the constraints from SNe. The middle curve shows a line of constant d_L at $z = 1$ that agrees with the Λ CDM model; the two other curves produce a d_L that differs from the fiducial value by $\pm 1\%$. As the figures show, the lines of CMB and SNe parameter degeneracies run nearly parallel to each other; however, both of those degeneracies are nearly orthogonal to the direction of the parameter degeneracy in cluster abundance studies. In particular, the maximum allowed value of w , using both the CMB or SNe data, is $w \approx -0.8$; while this is reduced to $w \approx -0.95$ when the cluster constraints are added. Note that in Figure 10, we have assumed a fixed value of $h = 0.66$; however, we find that relaxing this assumption does not significantly change this conclusion. The CMB and SNe constraints depend more sensitively on h than the cluster constraints do: as a result, the confidence regions do not overlap significantly even in the three-dimensional (w, Ω_m, h) space.

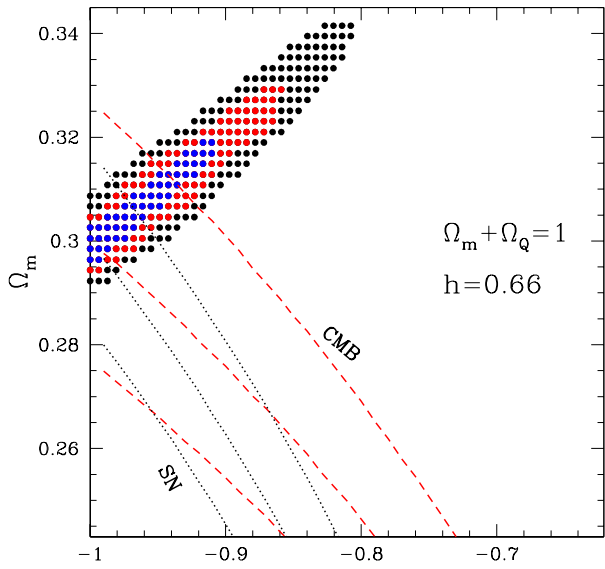


FIG. 10.— Confidence contours for a fixed $h = 0.66$ as in Figure 8, but zooming in for clarity. Also shown are combinations of w and Ω_m that keep the spherical harmonic index ℓ of the first Doppler peak in the CMB anisotropy data constant to within $\pm 1\%$ (dashed lines); and combinations that keep the luminosity distance to redshift $z = 1$ constant to the same accuracy.

The orthogonality of the cluster constraint to those from the other two methods can be understood based on the discussions in § 4.1. To remain consistent with the CMB and SNe Ia constraints, an increase in w must be coupled

with a decrease in Ω_m ; however, both increasing w and lowering Ω_m raises the number of detected clusters. To keep the total number of clusters constant, an increase in w must be balanced by an increase in Ω_m . Note that this statement is true both for the SZE and the X-ray surveys. Combining the cluster constraints with the CMB and SNe Ia constraints will therefore likely result in improved estimates of the cosmological parameters, and we do not expect this conclusion to rely on the details of the two surveys considered here.

7. CONCLUSIONS

We studied the expected evolution of galaxy cluster abundance from $0 \lesssim z \lesssim 3$ in different cosmologies, including the effects of variations in the cosmic equation of state parameter $w \equiv p/\rho$. By considering a range of cosmological models, we quantified the accuracy to which w , and other cosmological parameters can be determined in the future, using a 12 deg^2 Sunyaev-Zel'dovich Effect survey and a deep 10^4 deg^2 X-ray survey. In our analysis, we have assumed that the local cluster abundance is known accurately: we find that in practice, an accuracy of $\sim 5\%$ is sufficient for our results to be valid.

We find that raising w significantly flattens the redshift-distribution, which can not be mimicked by variations in either Ω_m , h , which affect essentially only the normalization of the redshift distribution. As a result, both surveys will be able to improve present constraints on w . In the $\Omega_m - w$ plane, both the SZE and X-ray surveys yield constraints that are nearly orthogonal to those obtained from the CMB anisotropy and high- z SNe. In combination with these data, the SZE survey can determine both w and Ω_m to an accuracy of $\approx 10\%$ at 3σ significance. Further improvements will be possible from the X-ray survey. The large number of clusters further alleviates the degeneracy between w and both Ω_m and h , and, as a result, the X-ray sample can determine w to $\approx 10\%$ and Ω_m to $\approx 1\%$ accuracy without relying on either the CMB or SN data, and to an accuracy of a few percent in combination.

Further work is needed to clarify the systematic uncertainties in our treatment, arising from the use of the Press-Schechter formalism, the analytic estimates of the scaling of the mass limits with cosmology, and our neglect of issues such as galaxy formation in the lowest mass clusters, or the accuracy to which the local abundance can be determined. However, our findings suggest that, in a flat universe, the cluster data lead to tight constraints on a combination of Ω_m and w , especially valuable because of its complementarity to those obtained from the CMB anisotropy or Hubble diagrams using SNe as standard candles.

We thank L. Hui for useful discussions, D. Eisenstein and D. Spergel for comments, and J. Carlstrom and the COSMEX team for providing access to instrument characteristics required to estimate the yields from their planned surveys. ZH is supported by the DOE and the NASA grant NAG 5-7092 at Fermilab, and by NASA through the Hubble Fellowship grant HF-01119.01-99A, awarded by the Space Telescope Science Institute, which is operated by the Association of Universities for Research in Astronomy, Inc., for NASA under contract NAS 5-26555. JJM is supported by Chandra Fellowship grant PF8-1003, awarded through the Chandra Science Center. The Chandra Sci-

ence Center is operated by the Smithsonian Astrophysical Observatory for NASA under contract NAS8-39073.

REFERENCES

- Arnaud, M. & Evrard, A.E. 1999, MNRAS, 305, 631
Bahcall, N.A., Ostriker, J. P., Perlmutter, S., & Steinhardt, P. J. 1999, Science, 284, 1481
Bahcall, N.A. & Fan, X. 1998, ApJ, 504, 1
Bautz, M.W., Pivovarov, M., Baganoff, G., Isobe, T., Jones, S.E., Kissel, S.E., Lamarr, B., Manning, H.L., Prigozhin, G.Y., Ricker, G.R., Nousek, J.A., Grant, C.E., Nishikida, D., Scholze, F., Thornagel, R., & Ulm, G. 1998, SPIE Proceeding, 3444, 210
Bond, J. R., & Myers, S. T. 1996, ApJS, 103, 41
Blanchard, A. & Bartlett, J.G. 1998, A&A, 332, L49
Bryan, G.L. & Norman, M.L. 1998, ApJ, 496, 80
Burles, S., & Tytler, D. 1998, ApJ, 499, 699
Caldwell, R.R., Dave, R. & Steinhardt, P.J. 1998, Ap&SS, 261, 303
Carlstrom, J.E., Joy, M.K., Grego, L., Holder, G.P., Holzappel, W.L., Mohr, J.J., Patel, S. & Reese, E.D. 1999, *Physica Scripta*, 60, in press (astro-ph/9905255)
Carroll, S., Press, W. & Turner, E. 1992, ARA&A, 30, 499
Chartas, G., Garmire, G., Nousek, J., Koch, S., Kissel, S., Prigozhin, G., & Bautz, M. 1998, SPIE Proceedings, 3444, 258
Eisenstein, D.J. 1996, PhD dissertation, Harvard University
Eisenstein, D.J. & Hu, W. 1998, ApJ, 504, L57
Evrard, A.E., Metzler, C.A. & Navarro, J.F. 1996, ApJ, 469, 494
Friedrich, P., Brauning, H., Burkert, W., Dohring, T., Egger, R., Hasinger, G., Oppitz, A., Predehl, P. & Trumper, J. 1998, SPIE Proceedings, 3444, 369
Gioia, I.M., Maccacaro, T., Schild, R.E., Wolter, A., Stocke, J.T., Morris, S.L. & Henry, J.P. 1990, ApJS, 72, 567
Gross, M.A.K., Zomerville, R.S., Primack, J.R., Holtzman, J. & Klypin, A. 1998, MNRAS, 301, 81
Holder, G.P., Mohr, J.J., Carlstrom, J.E., Evrard, A.E. & Leitch, E.M. 2000, ApJ, submitted (astro-ph/9912364)
Huey, G., Wang, L., Dave, R., Caldwell, R. R., & Steinhardt, P. J. 1999, Phys. Rev. D, 59
Lacey, C. & Cole, S. 1993, MNRAS, 262, 627
Lacey, C. & Cole, S. 1994, MNRAS, 271, 676
Lee, J. & Shandarin, S.F. 1999, ApJ, 517, L5
Metzler, C. A. 1998, ApJ, submitted, (astro-ph/9812295)
Mohr, J.J. & Evrard, A.E. 1997, ApJ, 491, 13
Mohr, J.J., Mathiesen, B. & Evrard, A.E. 1999, ApJ, 517, 627
Mohr, J.J., Carlstrom, J.E., Holder, G.P., Holzappel, W.L., Joy, M.K., Leitch, E.M. & Reese, E.D. 1999, Proceedings of the VLT Opening Symposium, Antofagasto, Chile, in press (astro-ph/9905256)
Mushotzky, R.F. & Scharf, C.A. 1997, ApJ, 482, 13
Peebles, P.J.E., 1980, *The Large Scale Structure of the Universe*, Princeton University Press: Princeton
Pen, U.-L. 1998, ApJ, 498, 60
Perlmutter, S. et al. 1999, ApJ, 517, 565
Press, W.H. & Schechter, P. 1974, ApJ, 193, 437
Press, W.H., Teukolsky, S.A., Vetterling, W.T. & Flannery, B.P., 1992, *Numerical Recipes in C: The Art of Scientific Computing*, 2nd Edition, Cambridge University Press: Cambridge
Raymond, J.C. & Smith, B.W. 1977, ApJS, 35, 419
Romer, A.K., Viana, P.T.P., Liddle, A.R. & Mann, R.G. 2000, ApJ, submitted (astro-ph/9911499)
Schmidt, B.P. et al. 1998, ApJ, 507, 46
Turner, M. S., & White, M. 1997, Phys. Rev. D, 56, 4439
Viana, P.T.P. & Liddle, A.R. 1996, MNRAS, 281, 323
Viana, P.T.P. & Liddle, A.R. 1999, MNRAS, 303, 535
Vikhlinin, A., McNamara, B.R., Forman, W., Jones, C., Quintana, H. & Hornstrup, A. 1998, ApJ, 503, 77
Wang, L., & Steinhardt, P. J. 1998, ApJ, 508, 483
Wang, L., Caldwell, R. R., Ostriker, J. P., & Steinhardt, P. J. 2000, ApJ, in press, (astro-ph/9901388)
White, M. 1998, ApJ, 506, 495